

Spectral Dynamic Causal Modelling of Resting-State fMRI: Relating Effective Brain Connectivity in the Default Mode Network to Genetics

Yunlong Nie¹, Laila Yasmin², Yin Song², Vanessa Scarapicchia³,
Jodie Gawryluk³, Liangliang Wang¹, Jiguo Cao¹, and Farouk S. Nathoo^{*,2}

¹Department of Statistics and Actuarial Science, Simon Fraser University

²Department of Mathematics and Statistics, University of Victoria

³Department of Psychology, University of Victoria

December 15, 2024

*Corresponding Author: Farouk S. Nathoo - nathoo@uvic.ca.

This research is supported by NSERC through the Discovery Grants program and through the Canada Research Chair in Biostatistics for Spatial and High-Dimensional Data; by CANSSI through a Collaborative Research Team Grant 'Joint Analysis of Neuroimaging Data: High-Dimensional Problems, Spatiotemporal Models and Computation'; by the University of Victoria through a UVic Internal Research Grant. Data collection and sharing for this project was funded by the Alzheimer's Disease Neuroimaging Initiative (ADNI) (National Institutes of Health Grant U01 AG024904) and DOD ADNI (Department of Defense award number W81XWH-12-2-0012).

Abstract

We conduct a novel imaging genetics study of the Alzheimer’s Disease Neuroimaging Initiative based on resting-state fMRI (rs-fMRI) and genetic data obtained from 112 subjects, where each subject is classified as either cognitively normal (CN), as having mild cognitive impairment (MCI), or as having Alzheimer’s Disease (AD). A Dynamic Causal Model (DCM) is fit to the rs-fMRI time series in order to estimate a directed network representing effective brain connectivity within the default mode network (DMN), a key network commonly known to be active when the brain is at rest. These networks are then related to genetic data and Alzheimer’s disease in the first genome-wide association study to use DCM as a neuroimaging phenotype.

Our proposed pipeline is comprised of four sequential analyses linked together with the objective of shedding light on the relationship between brain connectivity and genetics in relation to disease. In the first stage, we examine differences in effective brain connectivity across disease groups. In the second analysis we relate the probability of disease to genetics and obtain a set of priority single-nucleotide polymorphisms (SNPs) potentially related to disease. In the third analysis we investigate how effective brain connectivity is related to the set of priority SNPs obtained in the second study. In the fourth and final analysis we examine longitudinal data on changes with respect to MCI and AD through a classifier in order to determine how well disease progression can be predicted from the combination of effective brain connectivity and genetic data. Our new pipeline for connectome genetics has general applicability and its specific application to the ADNI study motivates a number of future studies in this nascent area.

KEYWORDS: Alzheimer’s Disease, Bayes Factors, Connectome Genetics, Dynamic Causal Model, Imaging Genetics, Neuroimaging, Resting-State fMRI

1. INTRODUCTION

Imaging genetics is an important area of scientific investigation in the search for genetic biomarkers of neurodegenerative disease, and in increasing our understanding of the genetic basis of brain structure and function in health and disease. The development of analytical methods for the joint analysis of neuroimaging phenotypes and genetic data is an important area of statistical research with many challenges. Recent reviews are provided in Liu and Calhoun (2014) and also in Nathoo et al. (2018).

The subfield of connectome genetics involves the investigation of relationships between genetics and connectivity in the brain (Thompson et al., 2013). In this paper we examine the relationship between genetics and effective brain connectivity as measured by resting-state fMRI (rs-fMRI) within regions of the default mode network (DMN), with an emphasis on the study of Alzheimer’s disease (AD).

AD is a neurodegenerative disorder characterized by cognitive decline and progressive dementia and is thought to be caused by aberrant connections between cerebral regions involved in cognitive functioning (Li et al., 2013). The DMN consists of a set of brain regions that tend to be active in resting-state, when a subject is mind wandering with no intended task. In this state DMN regions will exhibit low frequency signals that tend to couple together. It is a key member of a number of resting-state networks which have been studied over the last 10 years and is believed to be involved in the function of consciousness.

Previous literature focussing on AD has found alterations to both effective and functional resting-state connectivity in the DMN (see e.g., Wu et al., 2011; Yang et al., 2013; Luo et al., 2018). Here, effective connectivity refers to the directed influence of one brain region on others (Friston 1994) while functional connectivity refers simply to the correlation between measured time series over different locations. For example, Zhong et al. (2014) conduct an rs-fMRI study and demonstrate changes in effective connectivity in the DMN for subjects with AD, while Dipasquale et al. (2015) apply high-dimensional independent component analysis (ICA) to an rs-fMRI study and demonstrate changes in functional connectivity in

subjects with AD.

In general, the resting-state paradigm in neuroimaging is considered useful for investigating the functional or effective connectivity of the brain in order to determine if it is altered in neurological disorders. Resting-state fMRI data are collected with the goal of evaluating the interaction between different areas of the brain, and one of our primary goals is to understand the relationship between this neuronal interaction in the DMN and genetic variables that are related to AD. Within this paradigm we consider effective connectivity between four regions of the brain, known to be involved in the DMN, namely, the medial prefrontal cortex (mPFC), the posterior cingulate cortex (PCC), the left and right intraparietal cortex (LIPC and RIPC) with Montreal Neurological Institute (MNI) locations depicted in Figure 1.

To date, a great deal of work in imaging genetics has focussed on the relationship between brain structure and genetics (see e.g., Stein et al., 2010; Hibar et al., 2011; Ge et al., 2012; Zhu et al., 2014; Greenlaw et al., 2017; Szefer et al., 2017; Lu et al., 2017). Studies examining the relationship between brain connectivity and genetics have been considered to a lesser extent. Our analyses involve estimating effective connectivity networks from rs-fMRI data using Dynamic Causal Modeling (DCM; Li et al., 2011; Friston et al., 2003; Friston et al., 2014; Razi et al., 2015; Friston et al., 2017), a state-space framework for inferring interaction between hidden neuronal states. The DCM framework leads to estimated directed networks and these networks are used as a neuroimaging phenotype in our genetic analyses.

Given a set of R brain regions, DCM in the case of fMRI models the haemodynamic response over these regions through a nonlinear state-space formulation with a model allowing for interaction between regions and with model parameters that characterize effective connectivity and, when relevant, how this connectivity is modulated by experimental inputs. In the case of resting-state fMRI with no experimental inputs the model can be expressed as (see, e.g., Razi et al., 2017)

$$\begin{aligned}\dot{\mathbf{x}}(t) &= \mathbf{A}\mathbf{x}(t) + \mathbf{v}(t) \\ \mathbf{y}(t) &= h(\mathbf{x}(t), \boldsymbol{\theta}) + \mathbf{e}(t)\end{aligned}$$

where $\mathbf{x}(t) = (x_1(t), \dots, x_R(t))'$ are latent variables used to represent the states of neuronal populations at some time t and $\dot{\mathbf{x}}(t)$ is a time derivative defining a differential equation approximating neuronal dynamics, with the $R \times R$ matrix \mathbf{A} approximating effective connectivity to first-order; $h(\mathbf{x}(t), \boldsymbol{\theta})$ is a nonlinear mapping from neuronal states to the haemodynamic response also depending on parameters $\boldsymbol{\theta}$ (see, e.g., Friston, 2007); $\mathbf{y}(t) = (y_1(t), \dots, y_R(t))'$ with $y_j(t)$ being a summary of the response obtained from all voxels within region j ; $\mathbf{v}(t)$ and $\mathbf{e}(t)$ represent state and measurement noise respectively.

For resting-state fMRI the DCM model can be fit in the time-domain using Bayesian filtering based on a mean-field variational Bayes approximation (see, e.g., Li et al., 2011) which involves inference on both model parameters and latent states. Alternatively, the model can be fit in the spectral domain using an approach known as spectral DCM (Friston et al., 2014). The latter approach involves relating the theoretical cross spectra associated with the dynamic model to the sample cross spectra in order to estimate parameters. More specifically, Friston et al. (2014) assume a parameterized power law form for the spectral densities of the noise terms in the state-space model and then express the empirical cross spectra as the sum of the theoretical cross spectra and measurement error. This formulation then yields a likelihood for the observed cross spectra depending on the time-invariant parameters but not depending on the latent variables $\mathbf{x}(t)$. The likelihood is then combined with a prior distribution for model parameters and an approximation to the associated posterior distribution for these parameters is obtained using variational Bayes. Interestingly, Razi et al. (2015) report simulation results that demonstrate estimators obtained from spectral DCM having higher accuracy (in the sense of mean-squared error) than those obtained from stochastic DCM. In addition, the former has a higher computational efficiency since estimation of the latent states is not required.

To our knowledge, ours is the very first genome-wide association study (GWAS) to use a DCM-based neuroimaging phenotype, and this is an innovative aspect of our analysis. Our use of this measure as a phenotype is justified by the work of Xu et al. (2017) who examine effective connectivity within the DMN using DCM and structural equation modelling in

a twin study based on rs-fMRI. These authors estimate the heritability of DMN effective connectivity to be 0.54. Their study provides evidence that there are genes involved in DMN effective connectivity. This analysis then paves the way for our study which aims at identifying the genetic signals that influence DMN effective connectivity. We do this within the context of disease by first using a GWAS to determine a priority set of SNPs that are most relevant to MCI and AD. Previous work in Glahn et al. (2010) use an extended pedigree design and rs-fMRI to examine genetic influence on functional connectivity within the DMN. Their study estimates the heritability of DMN functional connectivity to be 0.424 ± 0.17 and it also suggests that the genetic factors that influence DMN functional connectivity and the genetic factors that influence gray matter density in these regions seem to be distinct.

We conduct global tests of association between this multivariate phenotype and genetic variables using the Bayes factor (Kass and Raftery, 1995). While the Bayes factor is the gold standard for Bayesian hypothesis testing and it has seen application in statistical genetics (see e.g., Marchini et al., 2007), its use in imaging genetics has surprisingly not been previously considered, as far as we are aware. Thus this first use of the Bayes factor in imaging genetics is another innovative and original aspect of our analysis.

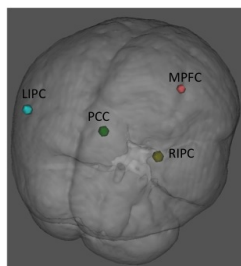


Figure 1: The locations of the four regions within the default mode network (DMN) examined in our studies: the medial prefrontal cortex (mPFC), the posterior cingulate cortex (PCC), the left and right intraparietal cortex (LIPC and RIPC) with MNI coordinates mPFC (3, 54, -2), the PCC (0, -52, 26), LIPC (-50, -63, 32) and RIPC (48, -69, 35).

Our proposed pipeline for preprocessing and analyzing the data is depicted in Figure 2. While it has been developed with our studies in mind, the pipeline can be applied more generally and is in and of itself a novel contribution of our work. In addition to genetic data preprocessing and neuroimaging data preprocessing and network estimation, the pipeline involves four studies. The first study examines the neuroimaging data in an effort to determine how the estimated effective connectivity networks vary by disease group. The second study examines the genetic data in order to determine which SNPs are most relevant to disease and to obtain a priority set of SNPs potentially related to disease. The third study relates the priority set of disease related SNPs found in the second study to effective brain connectivity networks in order to determine which SNPs have the highest evidence of being related to connectivity and what specific connections might be modulated by genetics. Finally, the fourth study examines how well disease progression can be predicted using the combination of genetic data and brain connectivity data through a set of classifiers. The overall goal of the four studies is to further our understanding of the relationship between information flow within the DMN and genetics within the context of disease, and to detect genetic signals exhibiting evidence of a relationship with brain connectivity and/or disease.

Stingo et al. (2013) focus on relating brain connectivity to genetics and develop a Bayesian hierarchical mixture model for studies involving fMRI data. The mixture components of the proposed model correspond to the classification of the study subjects into subgroups, and the allocation of subjects to these mixture components is linked to genetic covariates with regression parameters assigned spike-and-slab priors. There are four key distinctions between our work and that of Stingo et al. (2013). First, rather than the development of a single novel hierarchical model our emphasis is on the development of a pipeline that can be applied to understand the relationship between brain connectivity and genetics within the context of disease. Second, our analysis considers effective connectivity as opposed to functional connectivity in order to give a detailed picture of information flow within the brain and how this flow might be mediated by genetics. This is important as studies of effective connectivity in Alzheimer's disease are relatively few compared with studies of

functional connectivity. This relates to the third distinction, namely, that the focus of our study is on Alzheimer's disease as opposed to Schizophrenia. Fourth, our analysis involves the inclusion of a larger number of genetic variables; we consider 1,220,955 SNPs while Stingo et al. (2013) evaluate associations with 81 SNPs. It is worth clarifying again that our work involves the development of a pipeline and specific studies with analyses involving several innovations that are new to imaging genetics, while Stingo et al. (2013) have a primary focus on new methodology and the development of a novel Bayesian mixture model.

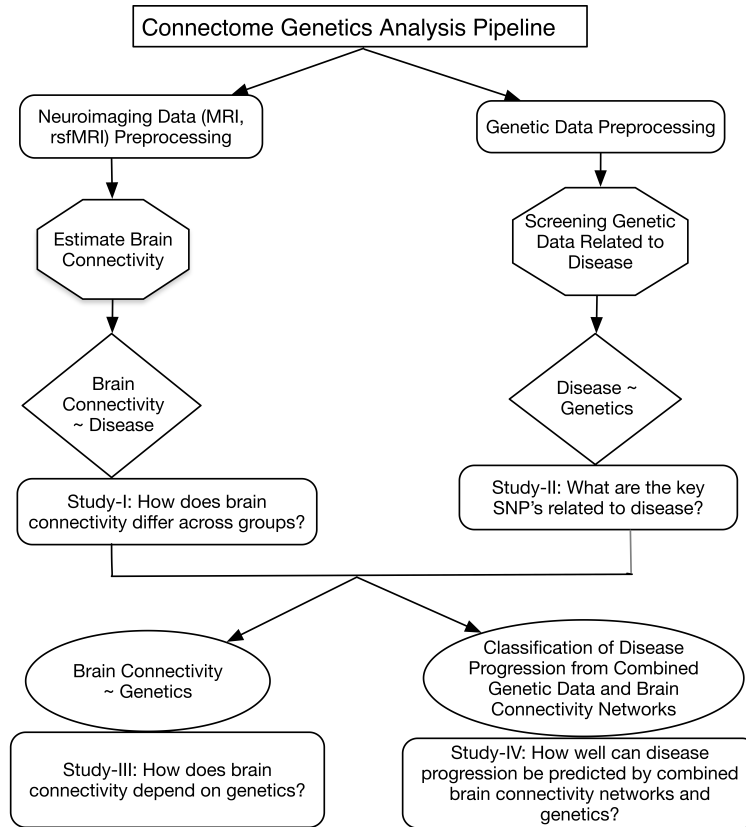


Figure 2: The sequence of genetic and neuroimaging data preprocessing steps, analysis, and questions addressed in the proposed connectome genetics pipeline.

Our study focuses on the relationship between genetics, more specifically, SNPs that are found related to AD and MCI, and effective brain connectivity in the DMN, a key resting-state network. The goal is to simultaneously investigate potential genetic biomarkers for early prediction of AD and MCI while trying to understand the mechanism by which these

potential biomarkers impact effective brain connectivity within the DMN. The four regions of interest considered in our work, depicted in Figure 1, are a subset of the regions that constitute the DMN.

These regions are also a subset of the DMN regions considered in the rs-fMRI study of Wu et al., (2011), which demonstrated altered DMN functional and effective connectivity in AD, and they are the same four DMN regions considered in the rs-fMRI study of Sharaev et al. (2016), which investigated internal DMN relationships.

Using rs-fMRI, genetic and demographic data from 112 subjects from the Alzheimer’s Disease Neuroimaging Initiative (ADNI) study, the primary questions/objectives that we wish to address are as follows: (1) we aim to investigate how effective brain connectivity in the DMN differs when comparing cognitively normal (CN) subjects, subjects with MCI, and subjects with AD; (2) beginning with a set of 1,220,955 SNPs from non-sex chromosomes, we wish to obtain a smaller set of priority SNPs that are potentially related to AD; (3) we examine how effective brain connectivity in the DMN depends on the priority SNPs that we find potentially related to AD in the second study; (4) we investigate the usefulness of genetic data and estimated effective brain connectivity networks for predicting disease progression towards AD. A key issue in the latter case is determining if the combination of genetic and brain connectivity data is more useful for predicting disease progression than either genetic data or brain connectivity data alone.

The remainder of the paper proceeds as follows. In Section 2 we discuss the neuroimaging and genetic data, summarize sample characteristics, the required preprocessing steps, and the construction of effective brain connectivity networks using DCM in more detail. In Section 3 we compare the brain networks across the three disease groups (CN, MCI, AD) in order to investigate how effective connectivity in the DMN differs across these groups. In Section 4 we examine how the genetic data are related to disease using a GWAS, and in doing so, obtain a priority subset of 100 SNPs for subsequent analysis. We also include this subset in a larger regression model and use the LASSO (Tibshirani, 1996; Friedman, 2010) to determine both the active SNPs as well as those SNPs that have the highest estimated

effect on the probability of disease. In Section 5 we relate the brain connectivity networks to the priority subset of SNPs determined in Section 4 using a multivariate linear model and the Bayes factor. Section 6 considers the problem of predicting disease progression, and we investigate the utility of genetic data and effective connectivity data for prediction while comparing a number of classification algorithms. The paper concludes in Section 7 with a summary of our findings.

2. DATA AND PREPROCESSING

Data used in the preparation of this article were obtained from the Alzheimer's Disease Neuroimaging Initiative (ADNI) database (adni.loni.usc.edu). The ADNI was launched in 2003 as a public-private partnership, led by Principal Investigator Michael W. Weiner, MD. The primary goal of ADNI has been to test whether serial magnetic resonance imaging (MRI), positron emission tomography (PET), other biological markers, and clinical and neuropsychological assessment can be combined to measure the progression of mild cognitive impairment (MCI) and early Alzheimer's disease (AD). For up-to-date information, see www.adni-info.org. ADNI is an ongoing, longitudinal, multicenter study designed to develop clinical, imaging, genetic, and biochemical biomarkers for the early detection and tracking of AD.

The selection criteria for our sample is as follows. We first begin with ADNI2 subjects (1437 at this stage) and considered those subjects with genome-wide SNP data (774 left at this stage) and also with at least one resting-state fMRI scan at 3T (112). This leads to 112 subjects comprising 37 CN, 63 MCI and 12 AD subjects, with these subjects having a mean age of 73.8 years with the range being 56.3-95.6 years, 46 of these subjects being male, 5 being left-handed, and with education measured in years ranging from 11 to 20. Table 1 displays several summary statistics associated with our sample including a summary on the APOE gene.

The APOE gene is a known genetic determinant of AD risk and individuals carrying the $\epsilon 4$ allele are at increased risk of AD (see, e.g., Liu et al. 2013). Table 1 summarizes the

number of APOE ϵ 4 alleles for the subjects in each disease category. In line with expectations from the literature, a signal from the APOE gene appears to be present in the data with the AD group having a higher percentage of subjects with at least one ϵ 4 alleles.

Table 1: Distribution of demographic variables across disease groups within our sample of 112 subjects. The p-values in the final column are based on a one-way ANOVA for continuous variables and a Fisher’s exact test for categorical variables.

		AD	MCI	N	p-value
n		12	63	37	
GENDER (% of group)	Female	8 (66.7)	34 (54.0)	23 (62.2)	0.640
	Male	4 (33.3)	29 (46.0)	14 (37.8)	
HAND (% of group)	Left	1 (8.3)	2 (3.2)	2 (5.4)	0.507
	Right	11 (91.7)	61 (96.8)	35 (94.6)	
Age - mean (sd)		75.82 (7.91)	72.70 (7.66)	75.22 (6.68)	0.165
EDUCATION - mean (sd)		16.33 (2.53)	16.06 (2.66)	16.30 (2.21)	0.874
APOE ϵ 4 Alleles (% of group)	Zero	1 (8.3)	35 (55.6)	24 (64.9)	0.0052
	One	9 (75.0)	22 (34.9)	12 (32.4)	
	Two	2 (16.7)	6 (9.5)	1 (2.7)	

Diagnostic classification of AD participants was made by ADNI investigators according to diagnostic criteria for probable AD established by the National Institute of Neurological and Communicative Disorders and Stroke and the Alzheimer's Disease Related Disorders Association (NINCDS-ADRA; McKhann et al., 1984). Participants in the AD cohort also exhibited abnormal memory function on the Logical Memory II subscale of the revised Wechsler Memory Scale, a Mini Mental State Exam (MMSE) between 20 and 26 (inclusive), and a Clinical Dementia Rating of 0.5 (very mild) or 1 (mild). All control participants were free of memory complaints and deemed cognitively normal based on clinical assessments by

the site physician showing an absence of significant impairment in cognitive functioning and performance of daily activities. Participants in the control cohort also exhibited normal memory function on the Logical Memory II subscale of the revised WMS, a MMSE score between 24 and 30 (inclusive), and a Clinical Dementia Rating of 0. For more information on group classifications, including all additional eligibility criteria, please consult the ADNI2 procedures manual (ADNI, 2008).

Our analysis uses rs-fMRI data from the baseline scan within ADNI2 for each subject. MRI for these subjects are T1-weighted images with the strength of magnetic field being 3T. MRI data were downloaded with permission from the ADNI. All images were acquired on 3.0 Tesla Philips MRI scanners across 10 North American acquisitions sites according to the standardized ADNI protocol. Whole-brain anatomical MRI scans were acquired sagittally, with a T1-weighted MPRAGE sequence, with the following parameters: 1.2 mm slice thickness, 256 by 256 by 170 acquisition matrix, echo time (TE) of 3 ms, in-plane voxel dimension of 1 mm², repetition time (TR) of 7 ms, and flip angle of 9. Functional MRI scans were obtained during resting-state; participants were instructed to lay quietly in the scanner with their eyes open. Resting state fMRI scans were obtained with a T2*-weighted echo-planar imaging sequence with the following parameters: 140 volumes, 64 by 64 by 48 acquisition matrix (voxel size = 3.3 mm³), TE of 30 ms, TR of 3000 ms, and flip angle of 80 degrees.

The freely available software package PLINK (Purcell et.al., 2007) was used for genomic quality control. The genetic data are SNPs from non-sex chromosomes, i.e., chromosome 1 to chromosome 22. SNPs with minor allele frequency less than 5% are removed as are SNPs with a Hardy-Weinberg equilibrium p-value lower than 10⁻⁶ or a missing rate greater than 5%. After preprocessing we are left with 1,220,955 SNPs for each of the 112 subjects.

2.1 rs-fMRI Data Preprocessing and Network Construction

The fMRI and anatomical data are pre-processed using a combination of the FSL software (available at <http://fsl.fmrib.ox.ac.uk/fsl/fslwiki/>) and the SPM12 software (available at <http://www.lion.ucl.ac.uk/spm/software/spm12/>). Non-brain tissue in

the raw T1 images is removed using the automated Brain Extraction Tool (Smith, 2002), followed by manual verification and optimization for each subject. BOLD data preprocessing was performed in FSL's FEAT as follows: each functional image was motion corrected and registered to their high-resolution T1 structural image that was linearly registered to standard stereotaxic space using a 12 degree of freedom transformation. A non-linear registration of the structural image to standard stereotactic space was also applied to account for potential local deformations in brains of the patient group. Each subject's imaging data are normalized to a standardized space defined by a MNI template brain.

The DMN includes the posterior cingulate cortex/precuneus (PCC), medial prefrontal cortex (mPFC), bilateral inferior parietal lobule (IPL), and other regions including the inferior temporal gyrus. To estimate effective connectivity within the four regions of the DMN depicted in Figure 1, we use spectral DCM as implemented in SPM12. BOLD time series from the DMN regions of interest are obtained by extracting time series from all voxels within an 8mm radius of the associated MNI coordinate, and then applying a principle component analysis and extracting the first eigenvariate. The result is a single representative time series for each region of interest. This procedure is repeated to obtain a collection of four time series for each of 112 subjects. An example of the resulting data for a single subject is depicted in Figure 3. A 16-parameter graph with weights representing effective connectivity between and within regions is then estimated for each subject. The imaging preprocessing pipeline is summarized in Figure 4.

We fit the DCM in SPM12 with the option of one state per region and with the model fit to the cross spectral density (spectral DCM).

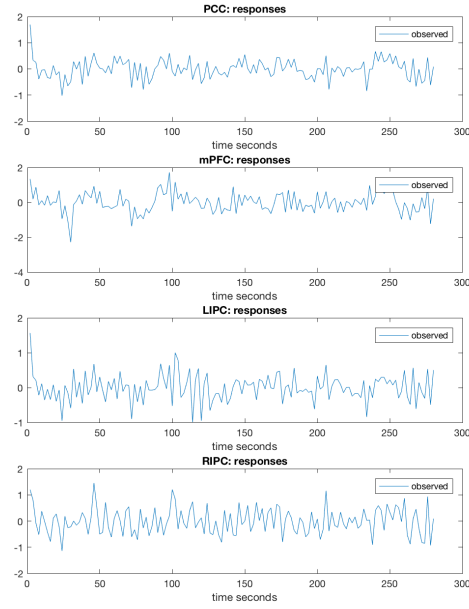


Figure 3: An example of the rs-fMRI data used to estimate the effective connectivity network for a single subject from the four regions of interest (PCC, mPFC, LIPC, RIPC).

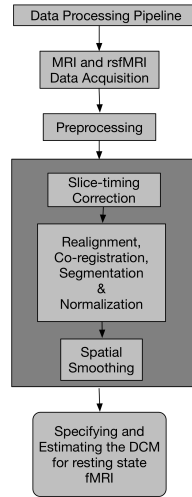


Figure 4: The steps involved in preprocessing the fMRI data and obtaining an effective brain connectivity network.

3. STUDY I: EFFECTIVE CONNECTIVITY BY DISEASE GROUP

Having estimated effective connectivity networks for each subject, the connectivity weights for all subjects are averaged within each of the three disease groups (CN, MCI, AD) and the resulting group-averaged effective connectivity networks are depicted in Figure 5. Weights having larger magnitude correspond to a stronger time-lagged dependence from one region to another or to itself. Beginning with the average point estimates of connectivity and examining how these estimates vary across groups, we note that the average estimated connection (standard deviation of the average) from RIPC to LIPC is higher for subjects with AD, 0.396 (0.155), when compared with subjects having MCI, 0.097 (0.054), and NC subjects, 0.067 (0.065). Similarly, the average estimated connectivity from PCC to MPFC is higher for AD subjects 0.272 (0.182) than MCI 0.00 (0.065) and NC -0.048 (0.056) subjects. These point estimates suggest that the posterior distributions of the DCM weights for AD subjects may be shifted away from the posterior distributions obtained from the non-AD subjects though the degree of variability (as seen from the standard deviation of the mean) seems to preclude any strong statements on group differences here. The greater average estimated connectivity in the AD group relative to the MCI and CN groups might reflect compensatory processes occurring even at rest. Again, the degree of posterior variability here precludes any strong statements on group differences.

To explore the preceding issue more formally, we next fit a set of 16 linear models where each model corresponds to one edge in the network, and the response for each regression model is the value associated with that edge as estimated by spectral DCM. Disease group (CN/MCI/AD) is included in the model as a categorical variable, and additional variables representing age, gender, right/left handedness, and education are included to adjust for potential confounding. An F-test is conducted at each edge to assess the significance of disease on effective connectivity at that given edge. The null hypothesis corresponds to the case where the population mean effective connectivity does not depend on disease status. That is, the case where the strength of connection is not related to disease. In our case

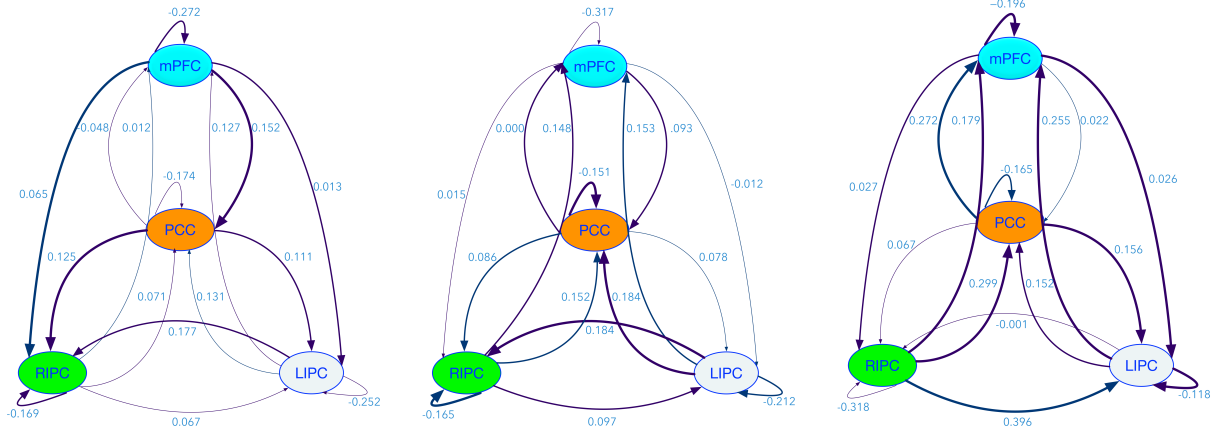


Figure 5: Average estimated connectivity weights for each of the three groups, left to right: normal controls, mild cognitive impairment, Alzheimer's disease.

the smallest p-values across the network correspond to $p = 0.081$ for the connection from RIPC to LIPC, and $p = 0.087$ for the connection from PCC to mPFC. After accounting for multiple comparisons at all edges, the false discovery rate (FDR) corrected p-values are depicted as a network in Figure 6. The FDR corrected p-values are $p = 0.696$ (RIPC \rightarrow LIPC) and $p = 0.696$ (PCC \rightarrow mPFC). From these values and Figure 6 it appears as though the data are not incompatible with the null hypothesis that the network connections do not differ across disease groups. Nevertheless, the RIPC \rightarrow LIPC and PCC \rightarrow mPFC connections may be of interest from an exploratory standpoint given the point estimates and their relative differences for the AD group.

4. STUDY II: RELATIONSHIP BETWEEN DISEASE AND GENETICS

Beginning with the 1,220,955 SNPs discussed in Section 2, we conduct a genome-wide association study (GWAS) with the goal of identifying a smaller subset of SNPs that are related to disease (CN/MCI/AD). A multinomial logistic regression with disease category as the response is fit for each SNP to assess that SNP's marginal association with disease after adjusting for covariates representing age, sex, right hand or left hand, and education. SNPs are included in the model as the number of a particular allele so that a SNP's effect on the log-odds ratio is additive. We sort the SNPs by the resulting p-values from a likelihood ratio

test, where the null hypothesis corresponds to the case where the probability distribution of disease does not depend on the given SNP. A subset of the top 100 SNPs is selected based on this ranking. The distribution of p-values by chromosome and the cut-off for selecting the best subset of 100 SNPs is depicted in Figure 7.

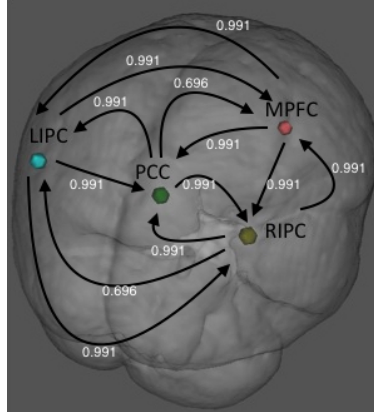


Figure 6: Network of FDR adjusted p-values from an analysis of covariance testing for the effect of disease group on edge weight while adjusting for age, gender, right/left hand, and education. FDR adjusted p-values for connections between any node and itself (self-connections) are computed but not displayed. The self-connections have FDR adjusted p-values 0.991 (LIPC), 0.991 (RIPC), 0.991 (PCC) and 0.991 (mPFC).

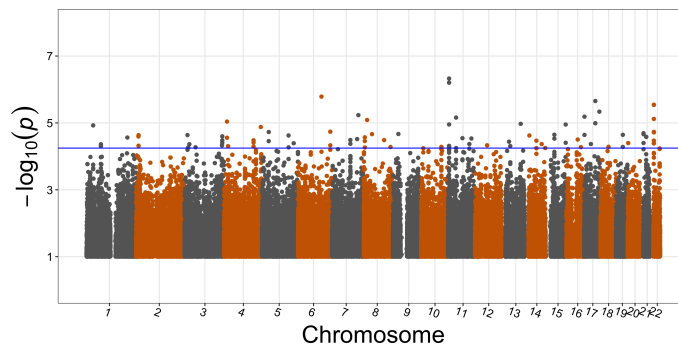


Figure 7: The p-values associating disease status with SNPs adjusting for age, sex, right or left hand and education. The blue line represents the cutoff used to obtain the top 100 SNPs.

To jointly assess the effect of the 100 priority SNPs, we include these variables along with covariates representing age, sex, right hand or left hand, and education and the disease status (CN/MCI/AD) as the response in a new symmetric multinomial logistic regression with LASSO penalty to jointly identify the SNPs that are most related to disease. The glmnet software (Friedman et al., 2010) is used to fit the LASSO penalized symmetric multinomial logistic regression model, where each class is represented by a linear model on the log-scale and the penalty allows for redundancies so that all levels of the response have an associated parameter in the model. The LASSO penalty parameter is selected using 10-fold cross validation. The estimated coefficients are summarized in Figure 8. The values represent how a unit increase in the coded allele will increase the log-odds ratio for a particular category of disease (NC/MCI/AD).

For each of the three disease categories (CN, MCI, AD), the top five SNPs selected based on the magnitude of their estimated LASSO coefficients are listed in Table 2. These findings suggest that SNPs kgp5568290, rs7617199 and kgp239829 have the largest estimated effects on the log-odds of AD.

While Table 1 indicates a potential APOE signal in our data from the $\epsilon 4$ allele, we note that there are no APOE SNPs in our subset of the top 100. Our data have two SNPs rs769449 and kgp2187574 that are located within the range of APOE (chr19:45409039, chr19:45412650). The individual associations between these two SNPs with the disease are not found to be significant, where the specific results are $p = 0.07$ for rs769449 and $p = 0.57$ for kgp2187574. As a result, neither of these two APOE SNPs are within the top 100 SNPs that we have identified and included in the larger model as their rank is quite low. If we define APOE related SNPs as those within a 1 million base pair range of APOE, we find 503 SNPs with p-values between 0.0005 and 0.99. In this case none of these 503 SNPs fall within the top 100 SNPs, though the highest rank among these is a rank of 1002 obtained by SNP kgp3912453. Given this, we look for more SNPs that might not be in the neighborhood of APOE, but may still be related to the APOE SNPs. To do this we start with the top 100 SNPs that are associated with disease status and we correlate them with

the first principal component obtained from those 503 SNPs that are in the 1 million base pair window of APOE. In this case the largest correlation is only about 0.28. As a result, there are no APOE SNPs in our subset of the top 100, though the highest ranking APOE SNP is kgp3912453 which obtains a rank of 1002 based on a p-value of 0.0005.

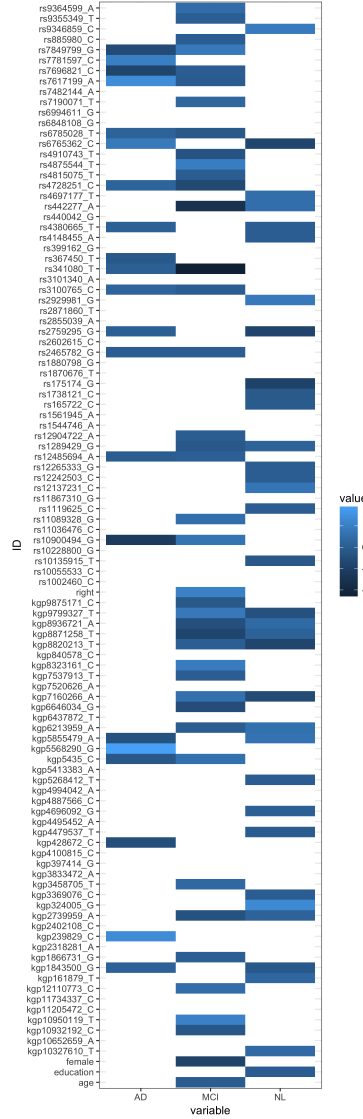


Figure 8: The coefficients estimated using LASSO-penalized multinomial logistic regression associating disease status with the top 100 significant SNPs adjusting for age, sex, right or left hand and education. White cells correspond to variables that have been deselected by the LASSO. The variable name consists of the SNP id and its corresponding coded allele.

CN - Top SNPs		MCI - Top SNPs		AD - Top SNPs	
ID	$\hat{\beta}$	ID	$\hat{\beta}$	ID	$\hat{\beta}$
kgp324005_G	1.26	rs341080_T	-2.39	kgp5568290_G	1.88
rs175174_G	-0.93	rs442277_A	-1.62	rs7617199_A	1.36
rs9346859_C	0.90	kgp10950119_T	1.07	kgp239829_C	1.33
rs2759295_G	-0.86	rs4875544_T	0.96	rs10900494_G	-1.21
rs2929981_G	0.83	kgp8323161_C	0.92	rs7781597_C	1.00

Table 2: Table of estimates showing the top five SNPs for each disease category along with the estimated regression coefficient from multinomial logistic regression with LASSO penalty.

5. STUDY III: RESTING-STATE BRAIN CONNECTIVITY BY GENETICS

We relate the resting-state effective connectivity networks estimated using DCM in Section 2.1 to each of the 100 priority SNPs most related to disease identified as part of the GWAS in Section 4 using the multivariate approach proposed in Marchini et al. (2007). This approach tests for SNP effects on a multi-dimensional phenotype using the Bayes factor. The test is based on a multivariate linear model

$$\mathbf{y}_i = x_i \boldsymbol{\beta} + \mathbf{e}_i, \quad \mathbf{e}_i \stackrel{iid}{\sim} N_{16}(0, \Sigma),$$

where $\mathbf{y}_i = (y_{i_1}, \dots, y_{i_{16}})^T$ denotes the vector of residual adjusted brain connectivity edge weights for the i th individual. Prior to fitting the multivariate model, adjusted connectivity is calculated by subtracting a baseline term based on linear regression estimates of an overall mean and the effects of covariates sex, age, left or right hand and education; x_i represents the number of a particular allele for a given SNP for the i^{th} individual; $\boldsymbol{\beta} = (\beta_1, \dots, \beta_{16})^T$ are the parameters that characterize the manner in which this SNP relates to the effective connectivity network; $\mathbf{e}_i = (e_{i_1}, \dots, e_{i_{16}})^T$ is the error term. An inverse Wishart prior $IW(c, Q)$ prior is assigned to the error covariance matrix Σ and a Gaussian prior is assigned to $\boldsymbol{\beta}$ as in Marchini et al. (2007).

The Bayes factor is computed to test the null hypothesis $H_0: \boldsymbol{\beta} = \mathbf{0}$ against H_1 :

$\beta \neq \mathbf{0}$, where the Bayes factor is defined by the ratio of marginal likelihoods $\text{BF} = m(\mathbf{y}|H_1)/m(\mathbf{y}|H_0)$, and quantifies the strength of evidence in favour of H_1 ; that is, the hypothesis that at least one network edge depends on the included SNP. The model is fit and the Bayes factor computed separately for each of the 100 priority SNPs, and based on this, the top 10 SNPs with the corresponding values of their Bayes factor are indicated in Table 2.

SNP id	BF
rs11036476	69.18
kgp239829	54.95
rs4910743	14.13
rs7482144	11.75
rs2855039	10.96
kgp10652659	10.23
kgp3458705	9.55
kgp5413383	6.61
kgp4994042	6.61
kgp161879	6.46

Table 3: The top 10 SNPs (based on the value of the Bayes factor) related to effective brain connectivity within the four regions of the DMN considered.

From Table 2 we can see that there are two distinct SNPs, rs11036476 (Bayes factor = 69.18) and kgp239829 (Bayes factor = 54.95), which give values of the Bayes factor indicating very strong evidence that effective connectivity in the DMN depends on these SNPs. We notice that among the top 10 SNPs listed in Table 2 that these two SNPs have Bayes factors that are noticeably larger than the other SNPs. Thus when we rank the SNPs according to the Bayes factor we see a rather large jump in the values of the Bayes factor when comparing the top two SNPs with the remaining SNPs on the list of the top 10. As demonstrated below, these SNPs both correspond to the same genetic signal from chromosome 11.

An important point to note is that SNP kgp239829 is also one of the top three SNPs found related to AD by LASSO in Study II, listed in Table 1, with estimated coefficient $\hat{\beta} = 1.33$ representing this SNP's effect on the log-odds ratio of AD. Our analysis thus suggests a SNP that is related to both AD and effective connectivity in the DMN.

To further investigate what specific connection in the networks depend on each SNP, we conduct a posthoc analysis independently for each of the top two, associating each edge value to a given SNP by fitting a linear regression of the edge value onto the SNP while also including covariates representing sex, age, left or right hand and education. The importance of the given SNP to each edge is then summarized through a p-value from an F-test.

Examining the networks for both SNPs and the p-values arising from the posthoc analysis relating each SNP to the 16 specific connections of interest, we find looking at both networks that these two SNPs are both strongly related to the same connections, namely, MPFC \rightarrow LIPC (rs11036476, p-value = 0.0055; kgp239829, p-value = 0.0052) and LIPC \rightarrow RIPC (rs11036476, p-value = 0.0058; kgp239829, p-value = 0.0063). We account for multiple comparisons across each network by computing FDR corrected p-values and these are depicted in Figure 9. For the strongest connections, the FDR corrected p-values are MPFC \rightarrow LIPC (rs11036476, p-value = 0.0462; kgp239829, p-value = 0.05) and LIPC \rightarrow RIPC (rs11036476, p-value = 0.0462; kgp239829, p-value = 0.05). We further notice that the networks of p-values for both of the top two SNPs are very similar. Investigating further, we find that both rs11036476 and kgp239829 are very close to each other on chromosome 11 and their sample correlation is very high $\hat{\rho} \approx 1$, so that both SNPs are in high linkage and represent the same genetic signal from chromosome 11 onto DMN connections MPFC \rightarrow LIPC and LIPC \rightarrow RIPC. As noted earlier, this same signal is also related to AD and thus suggests a potential a biomarker for AD that may also have a relationship to DMN effective connectivity at the two aforementioned connections.

It is also worth noting that the SNP with the third highest value of the Bayes factor rs4910743 (Bayes factor = 14.13) also exhibits a high correlation of $\hat{\rho} = 0.93$ with the top two SNPs and its network obtained from a posthoc analysis exhibits a pattern very similar

to that seen in Figure 9. This further suggests the same genetic signal potentially related to AD and DMN effective connectivity. We also note that while only one (kgp239829) of the top three SNPs listed Table 2 is also listed in Table 1 as having a large estimated effect on the probability of AD, this is likely the result of the well known property of the LASSO to choose one of a group of highly correlated predictors to include in the model. In this case LASSO has chosen kgp239829 to represent the chromosome 11 signal.

In summary, our analysis has detected a genetic signal from chromosome 11, SNP rs11036476 (Bayes Factor = 69.18), SNP kgp239829 (Bayes Factor = 54.95), and rs4910743 (Bayes factor = 14.13) all in high linkage exhibiting both a potential relationship to AD as well as a potential relationship to DMN connections MPFC \rightarrow LIPC and LIPC \rightarrow RIPC. As a result, it appears as though this genetic signal may modulate a path of information flow within the DMN from MPFC to RIPC through LIPC.

6. STUDY IV: CLASSIFICATION OF LONGITUDINAL DISEASE PROGRESSION FROM EFFECTIVE CONNECTIVITY NETWORKS AND GENETIC DATA

In our final study we examine longitudinal disease status data for each of the 100 out of 112 subjects included in our analyses that did not have AD (i.e., they were CN or MCI) at the time of their baseline rs-fMRI scan. In the ADNI2 study each subject’s disease status is monitored over time over a sequence of follow-up visits, with the number of visits varying from one to eight for the subjects included in our analyses. We define a subject to be a converter if their disease progressed, e.g., from CN to MCI, CN to AD or from MCI to AD during the course of follow-up. Subjects with only one visit (there are two such subjects) or those whose disease did not progress over multiple visits are called non-converters.

We investigate the development of a classifier that can predict disease progression with the goal of determining if the DMN effective connectivity networks from the baseline rs-fMRI scan and the genetic data (the subset of 100 SNPs from the GWAS of Study II) are useful as inputs into such a classifier. A primary question of interest in this study is whether the combination of brain imaging and genetic data yields a classifier that can perform in

predicting disease conversion better than the same classifier trained with genetic data only or brain imaging data only. In addition to SNP and estimated brain connectivity parameters, we include the age of subjects and the baseline disease state (either NC or MCI) as additional features in all of the classifiers. The data comprise 25 converters and 75 non-converters in total.

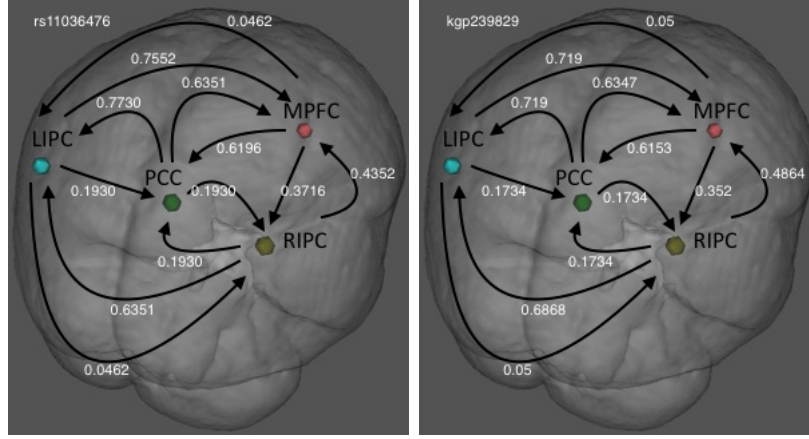


Figure 9: The FDR adjusted p-values obtained from F-tests associating effective connectivity between the brain regions of interest with each of the top two SNPs, rs11036476 (Bayes factor = 69.18) and kgp239829 (Bayes factor = 54.95), where the top 2 SNPs are identified by applying a multivariate linear model and the Bayes factor to the vector of residual DCM weights to each of the 100 SNPs identified as potentially related to disease in the GWAS of Section 2. The FDR adjusted p-values for connections between any node and itself (self-connections) are computed but not displayed. The self-connections for rs11036476 have FDR adjusted p-values 0.755 (LIPC), 0.272 (PCC), 0.372 (RIPC), 0.279 (MPFC); the self-connections for kgp239829 have FDR adjusted p-values 0.719 (LIPC), 0.291 (PCC), 0.354 (RIPC), 0.325 (MPFC).

We assess the accuracy of each classifier using five-fold cross-validation (CV) with the set of 100 subjects partitioned into five subsets. To keep the ratio of converters and non-converters roughly the same in the training and test sets, we randomly split the converters and non-converters into five folds separately, and we combine the i th fold of the converters

and the i th fold of the non-converters as the i th fold for the entire dataset. We report the average (over CV repetitions) test set sensitivity and test set specificity for all classifiers considered. The sensitivity is defined as the proportion of actual converters that are correctly identified by the classifier; the specificity is defined as the proportion of non-converters that are correctly identified by the classifier.

We consider classifiers that include some or all of the following inputs:

1. state: the disease state of the subject at baseline, either NC or MCI
2. age: the subject's age at baseline
3. brain connectivity: the estimated DCM effective connectivity network represented by a vector of 16 elements for each subject
4. genetic data: the top 100 SNPs obtained from Study II, indicated in Figure 8

We trained various classifiers with different sets of inputs:

1. completely random choice with no inputs (for baseline comparison)
2. age and state
3. age, state, and genetics
4. age, state, and effective brain connectivity
5. age, state, genetics and effective brain connectivity

For the case where the classifier uses age and state as the only inputs, we apply the following classification procedures: logistic regression, random forest (Liaw and Weiner, 2002), naive-Bayes (with and without a kernel), linear discriminant analysis (LDA) and a generalized additive model (GAM). For the cases where genetics and/or effective brain connectivity are also included as inputs, the number of predictors increases and we apply classifiers that are applicable to this setting, where the number of features is significantly

larger: regularized logistic regression with LASSO penalty, random forest, naive-Bayes (with and without a kernel), linear discriminant analysis (LDA), and generalized boosted machine (gbm). The results of comparing the different classifiers are summarized in Table 4, with the sensitivity and specificity for different classifiers listed in Table 4 all being based on a 0.5 cut-off value.

A very simple baseline for comparison is a classifier that simply chooses a class at random, and for such a classifier the sensitivity is 0.22 and the specificity is 0.78. Aside from this we evaluate four classes of classifier, the first with age and state, the second adding genetics to the first, the third adding effective brain connectivity to the first, the fourth adding both genetics and brain connectivity. In the first class the performance is quite poor as the sensitivity is far below baseline and it appears difficult to predict converters when only age and baseline state are used as inputs. For the remaining three classes we notice that the performance depends substantially on the type of classification algorithm used, and we also notice that in all three classes LDA and naive-Bayes achieve the best performance in terms of being able to predict disease progression.

The fact that it is LDA and naive-Bayes that perform best in all three classes suggests a genuine pattern with respect to the relative performance of algorithms for these data leaning towards simpler algorithms, perhaps because of the training set size. For these algorithms, we see that there is indeed an advantage to including both genetic data and brain connectivity data as inputs into the classifier, as the overall best performance is obtained when both brain connectivity and genetics are included. The LDA algorithm with age, state, genetics and brain connectivity appears to achieve the best performance overall, with a sensitivity of 0.56 and a specificity of 0.59. The ROC curves corresponding to the four LDA classifiers generated from varying the cut-off values are depicted in Figure 10.

A key result here is that the best classifier combines both brain connectivity and genetics (sensitivity = 0.56, specificity = 0.59) and that the ability of this same classifier to predict disease progression degrades when either brain connectivity is removed (sensitivity = 0.31, specificity = 0.61) or when genetics are removed (sensitivity = 0.28, specificity = 0.83).

The baseline classifier yields a sensitivity of 0.22 (with specificity of 0.78). We reiterate that the best performance was achieved when both genetic data and brain connectivity data were included as inputs into LDA. This suggests that the combination of both genetic and neuroimaging data may be useful for predicting disease progression.

Method	Predictor	Sensitivity	Specificity
Random Choice	NA	0.22	0.78
GAM	age+status	0.04	0.97
glm	age+status	0.04	0.97
LDA	age+status	0.04	0.97
naiveBayes	age+status	0.00	0.99
naiveBayes_kernel	age+status	0.04	0.99
randomForest	age+status	0.00	1.00
gbm	genetic+age+status	0.00	1.00
glmnet	genetic+age+status	0.00	1.00
LDA	genetic+age+status	0.31	0.61
naiveBayes	genetic+age+status	0.42	0.65
naiveBayes_kernel	genetic+age+status	0.00	1.00
randomForest	genetic+age+status	0.00	0.99
gbm	network+age+status	0.00	1.00
glmnet	network+age+status	0.00	1.00
LDA	network+age+status	0.28	0.83
naiveBayes	network+age+status	0.33	0.75
naiveBayes_kernel	network+age+status	0.32	0.74
randomForest	network+age+status	0.03	0.95
gbm	network+genetic+age+status	0.00	1.00
glmnet	network+genetic+age+status	0.00	1.00
LDA	network+genetic+age+status	0.56	0.59
naiveBayes	network+genetic+age+status	0.34	0.66
naiveBayes_kernel	network+genetic+age+status	0.00	0.97
randomForest	network+genetic+age+status	0.00	0.99

Table 4: Summary of average specificity and sensitivity for different classifiers with different predictors. The average specificity and sensitivity are based on a 0.5 cut-off value and the table entries are obtained by averaging five cross-validation errors.

7. DISCUSSION

We consider the relationship between genetics and rs-fMRI effective brain connectivity within the DMN in a study comprising 112 subjects classified as CN, MCI, or has having AD. In the current analysis we consider four specific regions within the DMN, namely, the mPFC, PCC, LIPC and RIPC. Effective connectivity networks are estimated using spectral DCM, which is appropriate when dealing with resting-state fMRI data. Our studies string together a number of simple yet effective analyses that have clear interpretations. A key innovation is the use of the Bayes factor for the first time in imaging genetics. In addition, ours represents the first ever use of DCM as a neuroimaging phenotype for a GWAS and our use of this phenotype is justified based on the twin study of Xu et al. (2017) who examine rs-fMRI effective connectivity within the DMN using DCM and structural equation modelling and estimate the heritability of DMN effective connectivity as 0.54.

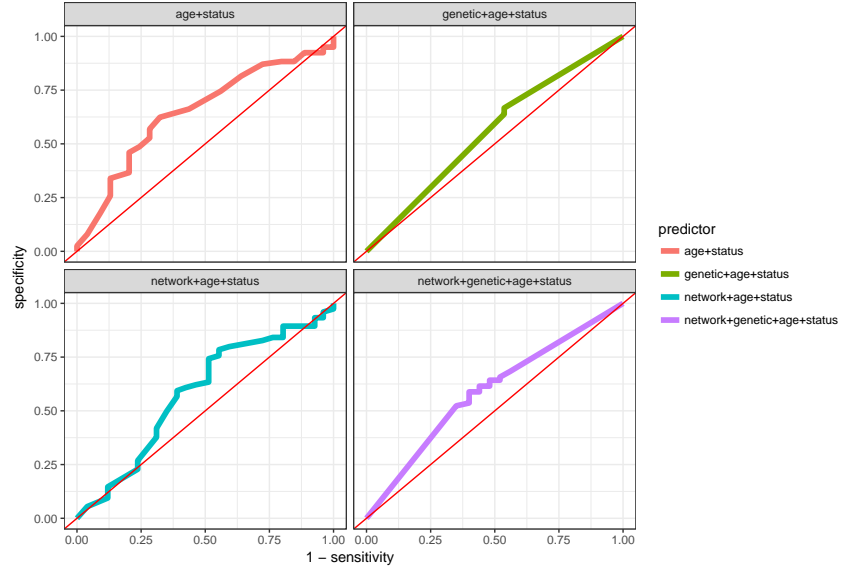


Figure 10: ROC curves for the four LDA classifiers considered in Study IV.

While data from the ADNI study have been examined intensively, our analyses of these data have revealed a number of interesting results. The most potentially interesting result is a genetic signal from chromosome 11, SNP rs11036476 (Bayes Factor = 69.18) and SNP kgp239829 (Bayes Factor = 54.95) exhibiting both a potential relationship to AD as well

as a potential relationship to DMN connections $MPFC \rightarrow LIPC$ and $LIPC \rightarrow RIPC$. As a result, it appears as though this genetic signal may modulate a path of information flow within the DMN from MPFC to RIPC through LIPC.

As far as we are aware, this is the first time this genetic signal has been identified on both DMN effective connectivity (Study III) and the probability of AD (Study II). Some caution is required here since the number of AD subjects in our study is low. The result for AD is based on LASSO with $n_{AD} = 12$ in the AD category for the multinomial logistic regression and $n = 112$ subjects in the model overall. The results for effective connectivity are based on the Bayes factor with $n = 112$.

A primary goal for follow-up work will involve studies that look at replicating the results found here. The results from Study II will be examined using a larger dataset with a targeted SNP analysis in order to determine if the chromosome 11 signal on the aforementioned DMN path can be replicated using a larger sample size.

Another approach to increasing the sample size is to extend our analysis to incorporate a longitudinal network analysis that uses rs-fMRI scans from multiple visits for each subject in the ADNI study. A primary challenge in this case is the need to accommodate within-subject clustering of the effective connectivity networks when relating these phenotypes to genetics in a repeated measures analysis. We are currently extending the analysis proposed here with longitudinal rs-fMRI data and random effects modelling.

The neuropathological mechanisms that underly the altered effective connectivity found here could be related to the usual hallmarks of AD. For example, amyloid plaques, neurofibrillary tangles and/or structural neurodegeneration may underly the altered connectivity and its observed association with genetics. Therefore, our current results also suggest follow-up studies examining measures of amyloid beta and tau (as measured in CSF or by PET imaging) and measures of brain structure (as measured by high resolution anatomical and diffusion tensor imaging) and the relationship between these measures and the genetic signal found in Studies II and III. Follow-up studies will also apply our pipeline to examine genetic effects on the effective connectivity in other resting-state networks relevant to AD such as

the Executive Control Network (Cai et al., 2017).

An alternative albeit more subtle way to increase the sample size associated with our analysis is to incorporate simulated rs-fMRI data based on a computer model of the brain. More specifically, a large number of subjects within the ADNI study do not have rs-fMRI data but instead have diffusion tensor magnetic resonance images (DTI) along with genetic data. The DTI for a given subject can be used to parameterize a complex computer model of neural activity that can be used in conjunction with appropriate forward modelling to simulate fMRI data and create a synthetic rs-fMRI dataset that is specific for that subject based on a model parameterized by their DTI. The result will be a larger sample size consisting of subjects with genetic data and either real rs-fMRI or synthetic computer model generated rs-fMRI data. We are currently investigating procedures for how to best simulate computer model data of the brain and methods for combining the computer simulated and real rs-fMRI data so as to achieve an optimal bias-variance tradeoff in the analysis of the combined data. This issue has received a great deal of attention in other areas such as climate modelling but has, as far as we are aware, never been considered for neuroimaging.

As fMRI reproducibility is a known issue (Eklund et al., 2016) and the results from GWAS in the absence of large sample sizes are also prone to similar problems arising from the small effects conferred by individual loci (Munafo and Flint, 2011), a priority at this point is investigating a potential theoretical explanation of our key results from Study III and designing candidate SNP studies to replicate them.

Finally, from a methodological perspective we note that our analysis in Study III is based on a two-stage approach and a problem with this approach is that the uncertainty associated with the parameters estimated in the first stage is not accounted for in the second stage analysis. Another problem with the two-stage approach is that the estimates of connectivity computed from each subject separately do not provide shrinkage. Shrinkage would offer the benefit of decreasing the variance of effective connectivity estimates compared with the current approach of estimating effective connectivity independently for each subject. Friston et al. (2015) discuss group analysis and shrinkage estimation for DCM and develop

an iterative approach where empirical priors from the second stage are used to iteratively optimize posterior densities over parameters at the first stage. Within our setup where interest lies in genetic effects one potential solution is to develop a fully Bayesian multi-subject model combining the DCM with a regression specification directly so that subject-specific parameters of the model representing neuronal connectivity are related to genetic variables through regression parameters modulating the dynamics of neural activity. Inference for this multi-subject genetic DCM model would then account for all sources of uncertainty, provide shrinkage in effective connectivity estimates and unify the two-stage analysis.

REFERENCES

- Cai, S., Peng, Y., Chong, T., Zhang, Y., M von Deneen, K., Huang, L., s Disease Neuroimaging Initiative, A. et al. (2017), “Differentiated Effective Connectivity Patterns of the Executive Control Network in Progressive MCI: A Potential Biomarker for Predicting AD,” *Current Alzheimer Research*, 14(9), 937–950.
- Dipasquale, O., Griffanti, L., Clerici, M., Nemni, R., Baselli, G., and Baglio, F. (2015), “High-dimensional ICA analysis detects within-network functional connectivity damage of default-mode and sensory-motor networks in Alzheimer’s disease,” *Frontiers in human neuroscience*, 9, 43.
- Eklund, A., Nichols, T. E., and Knutsson, H. (2016), “Cluster failure: why fMRI inferences for spatial extent have inflated false-positive rates,” *Proceedings of the National Academy of Sciences*, 113, 7900–7905.
- Friedman, J., Hastie, T., and Tibshirani, R. (2010), “Regularization paths for generalized linear models via coordinate descent,” *Journal of statistical software*, 33(1), 1–22.
- Friston, K. J. (1994), “Functional and effective connectivity in neuroimaging: a synthesis,” *Human brain mapping*, 2(1-2), 56–78.

- Friston, K. J., Harrison, L., and Penny, W. (2003), “Dynamic causal modelling,” *Neuroimage*, 19(4), 1273–1302.
- Friston, K. J., Kahan, J., Biswal, B., and Razi, A. (2014), “A DCM for resting state fMRI,” *Neuroimage*, 94, 396–407.
- Friston, K., Preller, K. H., Mathys, C., Cagnan, H., Heinzle, J., Razi, A., and Zeidman, P. (2017), “Dynamic causal modelling revisited,” *NeuroImage*, .
- Friston, K., Zeidman, P., and Litvak, V. (2015), “Empirical Bayes for DCM: a group inversion scheme,” *Frontiers in systems neuroscience*, 9, 164.
- Ge, T., Feng, J., Hibar, D. P., Thompson, P. M., and Nichols, T. E. (2012), “Increasing power for voxel-wise genome-wide association studies: the random field theory, least square kernel machines and fast permutation procedures,” *Neuroimage*, 63(2), 858–873.
- Glahn, D. C., Winkler, A., Kochunov, P., Almasy, L., Duggirala, R., Carless, M., Curran, J., Olvera, R., Laird, A., Smith, S. et al. (2010), “Genetic control over the resting brain,” *Proceedings of the National Academy of Sciences*, 107(3), 1223–1228.
- Greenlaw, K., Szefer, E., Graham, J., Lesperance, M., and Nathoo, F. S. (2017), “A Bayesian group sparse multi-task regression model for imaging genetics,” *Bioinformatics*, 33(16), 2513–2522.
- Hibar, D. P., Stein, J. L., Kohannim, O., Jahanshad, N., Saykin, A. J., Shen, L., Kim, S., Pankratz, N., Foroud, T., Huentelman, M. J. et al. (2011), “Voxelwise gene-wide association study (vGeneWAS): multivariate gene-based association testing in 731 elderly subjects,” *Neuroimage*, 56(4), 1875–1891.
- Jung, K., Friston, K. J., Pae, C., Choi, H. H., Tak, S., Choi, Y. K., Park, B., Park, C.-A., Cheong, C., and Park, H.-J. (2018), “Effective connectivity during working memory and resting states: A DCM study,” *NeuroImage*, 169, 485–495.

- Kass, R. E., and Raftery, A. E. (1995), “Bayes factors,” *Journal of the American Statistical Association*, 90(430), 773–795.
- Li, B., Daunizeau, J., Stephan, K. E., Penny, W., Hu, D., and Friston, K. (2011), “Generalised filtering and stochastic DCM for fMRI,” *Neuroimage*, 58(2), 442–457.
- Li, R., Yu, J., Zhang, S., Bao, F., Wang, P., Huang, X., and Li, J. (2013), “Bayesian network analysis reveals alterations to default mode network connectivity in individuals at risk for Alzheimer’s disease,” *PLoS One*, 8(12), e82104.
- Liaw, A., Wiener, M. et al. (2002), “Classification and regression by randomForest,” *R news*, 2(3), 18–22.
- Liu, C.-C., Kanekiyo, T., Xu, H., and Bu, G. (2013), “Apolipoprotein E and Alzheimer disease: risk, mechanisms and therapy,” *Nature Reviews Neurology*, 9(2), 106.
- Liu, J., and Calhoun, V. D. (2014), “A review of multivariate analyses in imaging genetics,” *Frontiers in neuroinformatics*, 8, 29.
- Lu, Z.-H., Khondker, Z., Ibrahim, J. G., Wang, Y., Zhu, H., Initiative, A. D. N. et al. (2017), “Bayesian longitudinal low-rank regression models for imaging genetic data from longitudinal studies,” *NeuroImage*, 149, 305–322.
- Luo, C., Li, Q., Lai, Y., Xia, Y., Qin, Y., Liao, W., Li, S., Zhou, D., Yao, D., and Gong, Q. (2011), “Altered functional connectivity in default mode network in absence epilepsy: a resting-state fMRI study,” *Human brain mapping*, 32(3), 438–449.
- Luo, X., Li, K., Jia, Y., Zeng, Q., Jiaerken, Y., Qiu, T., Huang, P., Xu, X., Shen, Z., Guan, X. et al. (2018), “Altered effective connectivity anchored in the posterior cingulate cortex and the medial prefrontal cortex in cognitively intact elderly APOE ϵ 4 carriers: a preliminary study,” *Brain imaging and behavior*, pp. 1–13.

- Marchini, J., Howie, B., Myers, S., McVean, G., and Donnelly, P. (2007), “A new multi-point method for genome-wide association studies by imputation of genotypes,” *Nature genetics*, 39(7), 906.
- McKhann, G., Drachman, D., Folstein, M., Katzman, R., Price, D., and Stadlan, E. M. (1984), “Clinical diagnosis of Alzheimer’s disease Report of the NINCDS-ADRDA Work Group* under the auspices of Department of Health and Human Services Task Force on Alzheimer’s Disease,” *Neurology*, 34(7), 939–939.
- Munafo, M. R., and Flint, J. (2011), “Dissecting the genetic architecture of human personality,” *Trends in cognitive sciences*, 15, 395–400.
- Nathoo, F. S., Kong, L., and Zhu, H. (2018), “A Review of statistical methods in imaging genetics,” *Canadian Journal of Statistics*, DOI: 10.1002/cjs.11487.
- Purcell, S., Neale, B., Todd-Brown, K., Thomas, L., Ferreira, M. A., Bender, D., Maller, J., Sklar, P., De Bakker, P. I., Daly, M. J. et al. (2007), “PLINK: a tool set for whole-genome association and population-based linkage analyses,” *The American Journal of Human Genetics*, 81(3), 559–575.
- Razi, A., Kahan, J., Rees, G., and Friston, K. J. (2015), “Construct validation of a DCM for resting state fMRI,” *Neuroimage*, 106, 1–14.
- Sharaev, M. G., Zavyalova, V. V., Ushakov, V. L., Kartashov, S. I., and Velichkovsky, B. M. (2016), “Effective connectivity within the default mode network: dynamic causal modeling of resting-state fMRI data,” *Frontiers in human neuroscience*, 10, 14.
- Smith, S. M. (2002), “Fast robust automated brain extraction,” *Human brain mapping*, 17(3), 143–155.
- Stein, J. L., Hua, X., Lee, S., Ho, A. J., Leow, A. D., Toga, A. W., Saykin, A. J., Shen, L., Foroud, T., Pankratz, N. et al. (2010), “Voxelwise genome-wide association study (vGWAS),” *Neuroimage*, 53(3), 1160–1174.

- Stingo, F. C., Guindani, M., Vannucci, M., and Calhoun, V. D. (2013), “An integrative Bayesian modeling approach to imaging genetics,” *Journal of the American Statistical Association*, 108(503), 876–891.
- Szefer, E., Lu, D., Nathoo, F., Beg, M. F., and Graham, J. (2017), “Multivariate association between single-nucleotide polymorphisms in Alzgene linkage regions and structural changes in the brain: discovery, refinement and validation,” *Statistical applications in genetics and molecular biology*, 16(5-6), 367–386.
- Thompson, P. M., Ge, T., Glahn, D. C., Jahanshad, N., and Nichols, T. E. (2013), “Genetics of the connectome,” *Neuroimage*, 80, 475–488.
- Tibshirani, R. (1996), “Regression shrinkage and selection via the lasso,” *Journal of the Royal Statistical Society. Series B (Methodological)*, pp. 267–288.
- Wang, Y., Risacher, S. L., West, J. D., McDonald, B. C., MaGee, T. R., Farlow, M. R., Gao, S., O’Neill, D. P., and Saykin, A. J. (2013), “Altered default mode network connectivity in older adults with cognitive complaints and amnesic mild cognitive impairment,” *Journal of Alzheimer’s disease*, 35(4), 751–760.
- Wu, X., Li, R., Fleisher, A. S., Reiman, E. M., Guan, X., Zhang, Y., Chen, K., and Yao, L. (2011), “Altered default mode network connectivity in Alzheimer’s disease? a resting functional MRI and Bayesian network study,” *Human brain mapping*, 32(11), 1868–1881.
- Xu, J., Yin, X., Ge, H., Han, Y., Pang, Z., Liu, B., Liu, S., and Friston, K. (2016), “Heritability of the effective connectivity in the resting-state default mode network,” *Cerebral Cortex*, 27(12), 5626–5634.
- Yan, H., Zhang, Y., Chen, H., Wang, Y., and Liu, Y. (2013), “Altered effective connectivity of the default mode network in resting-state amnesic type mild cognitive impairment,” *Journal of the International Neuropsychological Society*, 19(4), 400–409.

- Zhong, Y., Huang, L., Cai, S., Zhang, Y., von Deneen, K. M., Ren, A., Ren, J., Initiative, A. D. N. et al. (2014), “Altered effective connectivity patterns of the default mode network in Alzheimer’s disease: an fMRI study,” *Neuroscience letters*, 578, 171–175.
- Zhu, H., Khondker, Z., Lu, Z., and Ibrahim, J. G. (2014), “Bayesian generalized low rank regression models for neuroimaging phenotypes and genetic markers,” *Journal of the American Statistical Association*, 109(507), 977–990.